Rapid changes in mixed layer stratification driven by submesoscale instabilities and winds

JOURNAL OF GEOPHYSICAL RESEARCH, VOL. 115, C03017, doi:10.1029/2008JC005203, 2010

Rapid changes in mixed layer stratification driven by submesoscale instabilities and winds

A. Mahadevan,[1] A. Tandon,[2] and R. Ferrari[3]

Received 18 November 2008; revised 24 September 2009; accepted 7 October 2009; published 16 March 2010.

[1] Submesoscale eddies generated by baroclinic instability of upper ocean fronts lead to rapid restratification of the mixed layer on a time scale of days. This restratification can be opposed by a down-front wind stress (acting in the direction of the geostrophic velocity) that drives a surface Ekman flow from the dense side to the light side of the front to arrest the slumping of isopycnals. A scaling diagnostic is suggested to determine whether the effect of eddies or wind dominates under different conditions. Using a numerical model, we investigate the juxtaposition of submesoscale eddies and down-front winds acting on the mixed layer. By estimating the eddy-induced overturning stream function in the mixed layer, we separate the along- and cross-isopycnal fluxes of buoyancy associated with submesoscale mixed layer eddies and demonstrate the need for parameterization of the advective, along-isopycnal flux. Though the cross-front transport of buoyancy induced by the down-front component of the wind opposes restratification by mixed layer eddies, it becomes diminished as the eddies and growth of the frontal instability disrupt alignment between the wind and frontal axis.

Citation: Mahadevan, A., A. Tandon, and R. Ferrari (2010), Rapid changes in mixed layer stratification driven by submesoscale instabilities and winds, *J. Geophys. Res.*, *115*, C03017, doi:10.1029/2008JC005203.

1. Introduction

[2] The oceanic mixed layer (ML) is maintained through a competition between processes that mix away the stratification and those that restore it. Fluxes of momentum, heat, and salt, induced by winds, cooling, and evaporation at the air-sea interface, drive shear and convective instabilities that lead to turbulent mixing and reduce stratification. Conversely, precipitation and heating at the surface cause restratification. In this one-dimensional scenario, the ML deepens when surface waters become denser and trigger vertical mixing or when surface stresses drive shear instabilities. Conversely, it shallows when heating and precipitation reduce the surface density. Traditional ML models rely on such a one-dimensional budget for density to predict the evolution of ML depth and density.

[3] Recent work [e.g., *Thomas*, 2005; *Boccaletti et al.*, 2007] suggests that one-dimensional budgets that ignore the role of lateral instabilities in the ML are invalid whenever there are horizontal density gradients, as is nearly always the case in the real ocean [*Weller et al.*, 2004]. Consider the aftermath of a storm that led to vertical mixing and erased the vertical, but not the horizontal, stratification. The lateral gradients left behind undergo geostrophic adjustment [*Tandon and Garrett*, 1994] and then become baroclinically unstable, resulting in slumping of the vertical isopycnals back to the horizontal in a matter of days, i.e., a dynamical restratification [*Boccaletti et al.*, 2007; *Fox-Kemper et al.*, 2008]. Similarly, when winds blow over lateral density fronts, they can lead to restratification by advecting light water over dense or, conversely, destratification by advecting dense water over light. In all these scenarios, the change in vertical stratification is linked to lateral motions and cannot be predicted from a one-dimensional budget. More importantly, these processes are currently missing in ML models used for climate studies, raising serious issues about the skill of such models in predicting the ML structure, which in turn affects surface fluxes and the distribution of properties with depth.

[4] *Spall* [1995] pointed out that restratification at lateral fronts in the upper ocean is accelerated by frontogenesis. *Lapeyre et al.* [2006] considered a baroclinically unstable current with linear stratification over a depth of 3500 m. They found that the mesoscale geostrophic eddies generated by the instability resulted in sharp density fronts at the upper surface. The generation of the fronts, known as frontogenesis, was associated with an overturning circulation that slumped the fronts to the horizontal, resulting in rapid restratification. *Fox-Kemper et al.* [2008] showed that if a surface ML with weak stratification is included in the analysis, the surface fronts go unstable to ML submesoscale baroclinic instabilties that further accelerate the rate of slumping. These instabilities grow more rapidly (order of a

[1]Department of Earth Sciences, Boston University, Boston, Massachusetts, USA.
[2]Department of Physics and Department of Estuarine and Ocean Sciences, University of Massachusetts Dartmouth, North Dartmouth, Massachusetts, USA.
[3]Department of Earth, Atmospheric, and Planetary Sciences, MIT, Cambridge, Massachusetts, USA.

0148-0227/10/2008JC005203

day) and with smaller length scales (order of a kilometer) than baroclinic instabilities in the pycnocline [*Capet et al.*, 2008a, 2008b]. Their Rossby and Richardson numbers are close to one, and hence, they differ dynamically from interior mesoscale eddies [*Thomas et al.*, 2008]. Yet the role of submesoscale eddies in the mixed layer is, in some ways, analogous to that of mesoscale eddies in the midlatitude ocean pycnoclines. Ekman pumping steepens isoypycnals in the pycnocline by drawing them toward the surface at major fronts, while baroclinic instabilities lead to the formation of vigorous mesoscale (~100 km) eddies that tend to slump the warm water lenses [*Green*, 1970] and flatten the isopycnals. In climate models, the flux associated with pycnocline eddies needs to be parameterized in order to simulate major pycnocline fronts like the Antarctic Circumpolar Current and Western Boundary Currents [*Gent and McWilliams*, 1990]. Similarly, the flux associated with submesoscale mixed layer eddies (MLE) needs to be parameterized in order to simulate the evolution of stratification in a model that does not explicitly resolve dynamics at the submesoscale [*Fox-Kemper and Ferrari*, 2008].

[5] Observations by *Hosegood et al.* [2006] show that upper ocean fronts are often baroclinically unstable and exhibit variability at scales of the order of the ML deformation radius, the submesoscale (1–10 km). The instabilities eventually develop into MLE that rapidly restratify the ML in a few days [*Fox-Kemper et al.*, 2008]. Submesoscale MLE achieve restratification by driving a thermally direct overturning circulation that converts density gradients from the horizontal to the vertical. Numerical simulations show that the restratification by the MLE persists in the presence of diurnal cycling. Indeed, *Fox-Kemper et al.* [2008] suggest a parameterization for inclusion of restratification in the ML due to MLE. However, their work does not consider the effect of winds.

[6] Complementary observations by *Lee et al.* [2006] suggest that changes in stratification at ML fronts take the cue from wind conditions. Winds can both aid and destroy the stratification in the ML, depending on their orientation. When the wind stress has a component up front, it will advect lighter water over dense, restratifying the ML. The response to a wind stress with a down-front component is described by *Thomas* [2005] and *Thomas and Lee* [2005]. Down-front winds advect dense water over light, giving rise to an ageostrophic circulation which destroys the ML stratification and leads to intensification of the upper ocean front, thus increasing the available potential energy. *Thomas and Ferrari* [2008] showed that down-front winds can easily overcome the restratification ensuing from frontogenesis. However, their analysis did not consider restratification by MLE.

[7] MLE, up-front winds, and down-front winds thus give rise to three-dimensional processes that have opposing effects on the stratification within the ML. A priori, the combined effect of these two physical processes is not clear. One possibility is that down-front wind forcing suppresses MLE before they reach finite amplitude and thus obviates the need for parameterizing any effect of MLE whenever a down-front wind component is present. Another possibility is that the MLE completely counter the effect of down-front winds, resulting in a stationary front and obviating the need for parameterizing any of the two effects. Finally, the two processes might interact nonlinearly and require a complete revamping of our understanding of both effects. In summary, the interaction between MLE and winds, and the ensuing mixed layer stratification evolution, is not well understood.

[8] The goal of this study is to consider the combined effect of MLE and winds on the evolution of the ML stratification. Using a numerical model of a ML front that goes baroclinically unstable and generates MLE, we study the evolution of the ML in the absence of winds and in the presence of down-front and up-front winds. In order to quantify the relative contributions of MLE and winds to the ML evolution, we use the transformed Eulerian mean (TEM) framework, which allows a clean separation of the eddy fluxes due to instabilities versus those due to wind-forced motions. The problem with the traditional TEM framework is that it is not well defined in regions of weak stratification, a situation often encountered in our simulations and in the real ML. In response, we use a new formulation that remains valid in both stratified and unstratified environments.

[9] The paper is organized as follows. In section 2, we introduce the numerical model, and in section 3 we discuss the new TEM formulation. Discussion of the numerical results and their implications for our understanding of the competition between MLE and winds are in section 4. Finally, in section 5, we conclude by reviewing the importance of including lateral dynamics in models of the ML. Our work provides a road map on how to include the effect of MLE in the presence of winds, following the approach taken by *Fox-Kemper and Ferrari* [2008].

2. Modeling

[10] We use a three-dimensional ocean circulation model [*Mahadevan et al.*, 1996a, 1996b] to simulate ML instability as done by *Fox-Kemper et al.* [2008]. The fully nonhydrostatic Bousinesq equations are solved in a periodic reentrant channel in x bounded by walls at $y = 0$, L_y [*Mahadevan*, 2006]. The domain, $L_x \times L_y = 96 \times 192$ km^2 and 500 m deep, is initialized with a front centered at $y = L_y/2 = 96$ km within a ML of depth $H = 200$ m. We set $f = 10^{-4}$ s^{-1}. Initially, a very weakly stratified ML ($N^2 = 10^{-6}$ s^{-2}) overlies a pycnocline; N^2 attains a maximum value of 180×10^{-6} s^{-2} at 240 m depth and decreases to 10×10^{-6} s^{-2} at 500 m. A lateral density variation of 0.2 kg m^{-3} is prescribed within the ML as $\Delta\rho = 0.1 \tanh [0.03\pi(y - L_y/2)]$, where y is in km, and is linearly tapered to 0 within ±10 m of the ML base. The maximum lateral buoyancy gradient at the front is $b_y = -0.9 \times 10^{-7}$ s^{-2}. The horizontal grid resolution is 1 km, and in the vertical, 32 layers range in thickness from 2 m at the surface to 36 m at depth. In most of the wind-forced model runs, a constant wind stress is prescribed in the x direction according to $\tau^x = \tau_0 \cos\{[(y - 0.5L^*_y)/L^*_y]\pi\}$. It is tapered to 0 near the boundaries ($L^*_y = 0.9L_y$) to prevent Ekman pumping velocities at the walls. For all the simulations, we use the same values for diffusivity and viscosity. In the horizontal, $K_h = 1$ m^2 s^{-1}. In the vertical, $K_v = max\{K_{\max}[(1/2) + (1/2)\tanh((z + \delta_E)/\Delta)\pi], K_{\min}\}$, which transitions smoothly from $K_{\max} = 10^{-3}$ m^2 s^{-1} in the turbulent surface Ekman layer, which lies above the depth $\delta_E = (0.4/f)(\tau^x/\rho)^{1/2}$, to $K_{\min} = 10^{-5}$ m^2 s^{-1} in the

interior. Here $\Delta = 0.5\ \delta_E$ is a transition height and $z = 0$ is the surface. We find that the rate of stratification and the qualitative nature of our simulations do not change with a higher value of $K_{\max} = 10^{-2}$ m^2 s^{-1} or with a more gradual transition $\Delta = \delta_E$. Hence, all results presented are with $K_{\max} = 10^{-3}$ m^2 s^{-1}, $K_{\min} = 10^{-5}$ m^2 s^{-1}, and $\Delta = 0.5\ \delta_E$.

[11] We perform a number of numerical experiments to examine the competition between MLE in restratifying the ML and a down-front wind stress in destratifying it. We present results for wind stress $\tau_0 = 0$, $\tau_0 = 0.1$ N m^{-2}, $\tau_0 = 0.2$ N m^{-2}, and $\tau_0 = 0.3$ N m^{-2}. Two additional cases with up-front winds, $\tau_0 = -0.1$ N m^{-2} (not shown since the surface is quickly covered with light water) and a wind stress that alternates between up front and down front as $\tau_0 = 0.2 \sin(\pi\, t/10)$, where t is given in days, are implemented. We run the simulations for 45 days. Even though a sustained wind stress for such a period is unrealistic, the length of the model run enables us to explore the mechanisms at play.

3. Eddy-Induced Circulation and Fluxes at a Front

[12] The residual mean framework has been used to separate the advective and cross-isopycnal transport associated with eddies in the stratosphere [e.g., *Plumb*, 2002] and in the Southern Ocean [e.g., *Marshall and Radko*, 2003]. These studies rely on quasi-geostrophic (QG) scaling. Here we show that the residual mean approach retains its utility for a non-QG upper ocean front. Consider an infinitely long ML front aligned along the x direction with a negative buoyancy gradient in y, i.e., $b_y < 0$. (Buoyancy is $b \equiv g\rho'/\rho_0$, where ρ' is the deviation of density from a reference state ρ_0.) The geostrophic flow along x is baroclinically unstable. Our interest lies in determining the net circulation and rearrangement of buoyancy in the y-z plane, normal to the front and averaged in x.

[13] Using a decomposition of properties into a mean (averaged along x and denoted by an overbar) and fluctuations (denoted by a prime), the evolution equation for buoyancy becomes

$$\frac{\partial \overline{b}}{\partial t} + \overline{\mathbf{u}} \cdot \nabla \overline{b} = \frac{\partial \overline{b}}{\partial t} + J\left(\overline{\psi}, \overline{b}\right) = -\nabla \cdot \left(\overline{\mathbf{u}' b'}\right), \tag{1}$$

where J is the Jacobian operator and $\overline{\psi} \equiv -\int_0^z \overline{v}\, dz = \int_0^y \overline{w}\, dy$ is the overturning stream function associated with the along-front averaged velocity field. This is the classical Reynolds equation for turbulent flows. Following residual mean theory, the eddy buoyancy flux $\overline{\mathbf{u}' b'}$ is decomposed as the sum of skew flux $\mathbf{F}_{\text{skew}} \equiv \psi_e \hat{\mathbf{x}} \times \nabla \overline{b}$ directed along isopycnals (along b surfaces) and a residual flux $\mathbf{F}_{\text{res}}$. The divergence of the skew flux represents advection of mean buoyancy $\overline{b}$ by the eddy stream function ψ_e, i.e., $\nabla \cdot \mathbf{F}_{\text{skew}} = J(\psi_e, \overline{b})$. The challenge is to define an eddy stream function ψ_e such that $\mathbf{F}_{\text{skew}}$ captures the bulk of the eddy flux and $\mathbf{F}_{\text{res}} = \overline{\mathbf{u}' b'} - \psi_e \hat{\mathbf{x}} \times \nabla b$ is a small residual. We expect this to be possible in the present problem because the MLE perform an adiabatic rearrangement of buoyancy, and hence, the bulk of the eddy flux should be directed along isopycnals.

[14] Conventional definitions of ψ_e include $\psi_e = \overline{v' b'}/\overline{b}_z$ for the interior [*Andrews and McIntyre*, 1976] and $\psi_e = -\overline{w' b'}/\overline{b}_y$ for the boundary layer [*Held and Schneider*, 1999]. These forms become undefined if either $\overline{b}_y$ or $\overline{b}_z$ approaches zero, a situation often encountered in the ML [*Ferrari et al.*, 2008]. A more general definition was suggested by *Plumb and Ferrari* [2005] and *Cerovecki et al.* [2009]. It uses a coordinate stretching to account for the skewed (depth to length) aspect ratio. Following this suggestion, we scale our z coordinate by ϵ^{-1} ($\epsilon \ll 1$) and combine the previous forms for ψ_e to give

$$\psi_e = \epsilon \left(\frac{\epsilon\, \overline{v' b'}\, \overline{b}_z - \epsilon^{-1}\, \overline{w' b'}\, \overline{b}_y}{\overline{b}_y^2 + \epsilon^2\, \overline{b}_z^2} \right), \quad \epsilon \ll 1. \tag{2}$$

We choose $\epsilon = 10^{-3}$. The formulation of ψ_e is not sensitive to the choice of ϵ, as we verify for the range 10^{-2}–10^{-4}. The advantage of (2) is that it remains well defined in weakly stratified environments, unlike previous definitions, yet allows us to extract that part of the eddy flux which is directed along isopycnals, i.e., is adiabatic. In oceanographic applications, eddy slumping is mostly adiabatic, and ψ_e thus captures the majority of the eddy flux.

[15] The advantage of the residual mean decomposition of the eddy fluxes becomes apparent in terms of the buoyancy budget since (1) can be rewritten as

$$\frac{\partial \overline{b}}{\partial t} + J\left(\bar{\psi} + \psi_e, \overline{b}\right) = -\nabla \cdot \mathbf{F}_{\text{res}}. \tag{3}$$

This budget shows that the mean buoyancy $\overline{b}$ is advected both by the mean overturning stream function $\overline{\psi}$ and by a circulation induced by the eddy motions, ψ_e. To the extent that eddy fluxes are primarily directed along isopycnals, this advection captures the bulk effect of eddies on the mean buoyancy budget.

[16] At ML fronts, ψ_e leads to the slumping of fronts as a result of submesoscale baroclinic instabilities. This circulation is always thermally direct with light (warm) waters rising above dense (cold) waters. The eddy stream function competes with the mean overturning stream function driven by the winds, $\overline{\psi} \approx -\tau^x/\rho f$, which can be either thermally direct or indirect, depending on the sign of the wind stress. Whether restratification occurs or not depends on the overall transport and rearrangement of buoyancy by the residual circulation, i.e., the sum of the eddy and mean contributions, $\psi_r = \overline{\psi} + \psi_e$.

4. Results

[17] It is well known that whenever vertical mixing erases thermal wind balance at a front in the ML, the front undergoes geostrophic adjustment [*Tandon and Garrett*, 1995]. The adjustment results in minimal restratification. However, *Boccaletti et al.* [2007] show that if the front goes baroclinically unstable soon after the initial adjustment, it results in rapid slumping and restratification. The question remains as to whether the submesoscale baroclinic instabilities persist in the presence of winds, in particular, when winds are down front and act to maintain the verticality of the isopycnal surfaces at the front. The cancellation between processes could lead to the persistence of fronts, whereas the dominance of MLE would result in restratification of the ML.

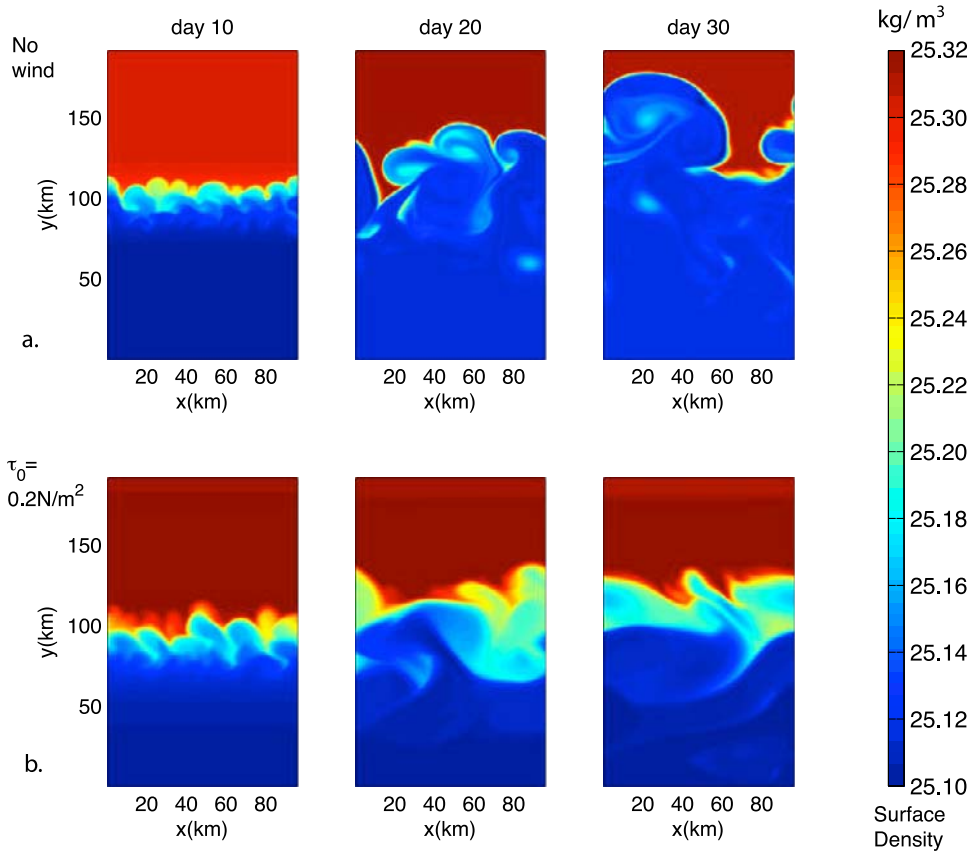

Figure 1. Time sequence of the surface density showing the evolution of MLE in the cases of (a) no wind and (b) $\tau_0 = 0.2$ N m^{-2}, where the wind blows from left to right. With the sustained down-front wind stress $\tau_0 = 0.2$ N m^{-2}, the growth of MLE is curtailed and restratification of the ML is prevented, as seen in the vertical sections of Figure 2.

[18] *Fox-Kemper et al.* [2008] show that the strength of the eddy-driven overturning stream function associated with MLE scales as $\psi_e \sim 0.06\, H^2\, \overline{b_y}/f$. The mean overturning stream function $\overline{\psi}$ is largely wind driven and follows the classical Ekman scaling $\overline{\psi} \sim -\tau_0/\rho f$. For down-front winds, $\overline{\psi}$ and ψ_e have opposite signs, implying opposing overturning circulations. We introduce the ratio $r \equiv |\overline{\psi}/\psi_e| = \tau_0/(0.06\rho H^2 \overline{b_y})$ to determine the dominance of destratification by down-front winds versus the restratification by MLE. For $H = 200$ m and $\overline{b_y} = -0.9 \times 10^{-7}$ s^{-2}, typical values for deep ML fronts at midlatitudes, the ratio $r = 1$ is achieved when $\tau_0 \approx 0.2$ N m^{-2}. In what follows, we show that this scaling estimate is roughly consistent with our model results. The growth of MLE is curtailed and restratification is restricted when $r \geq 1$ ($\tau_0 \geq 0.2$ N m^{-2} in this case), whereas the MLE and meandering front spread through the domain and generate a stable restratification throughout the region when $r < 1$. Whereas r is a scaling estimate based on initial conditions, the flux of buoyancy due to the wind- and eddy-driven circulation can vary in time as the front evolves and meanders. A more dynamic estimate that takes into account the ratio of wind-driven and eddy-driven buoyancy fluxes is $r_{\text{flux}} \equiv \langle\langle \tau_0 b_y \rangle\rangle / \langle\langle 0.06\rho H^2 b_y^2 \rangle\rangle$, where $\langle\langle\ \rangle\rangle$ denotes areal averaging over the surface, b_y is evaluated at the surface, and τ_0 is the wind stress in the x direction. When the front meanders, the wind-driven buoyancy flux depends on the alignment of the wind with the frontal axis.

[19] Before discussing the competition between MLE and winds, let us consider a simulation of a baroclinically unstable ML front in the absence of any wind forcing. The model domain is initialized with an east-west straight front over a 200 m deep ML, as described in section 2. The front develops submesoscale meanders and eddies that grow on a time scale of days to form larger eddies that fill the domain as the flow evolves (Figure 1a). Baroclinic instability and the ensuing MLE act to slump the density front and increase the stratification. From a potential vorticity (PV) perspective, the restratification results from advection of high PV (highly stratified) waters from the pycnocline into the ML, as described by *Boccaletti et al.* [2007] (see Figure 2a). Surface frontogenesis brought about by MLE also contributes to the development of stratification near the surface. But interestingly, the largest concentration of stratification is acquired at middepth in the ML. In this simulation without wind, the average N^2 in the 200 m deep ML increases from 10^{-6} s^{-2} to 10^{-5} s^{-2} and spreads through the 200 km horizontal domain in 40 days. The stratification generated is a factor of 10 larger than expected from geostrophic adjustment of the front, namely, $N^2 \sim (b_y)^2/f^2$ [*Tandon and Garrett*, 1995].

[20] Addition of a down-front wind stress results in advection of dense water over light and the destruction of stratification at the surface. Whether this results in an arrest of restratification by MLE depends on the strength of the

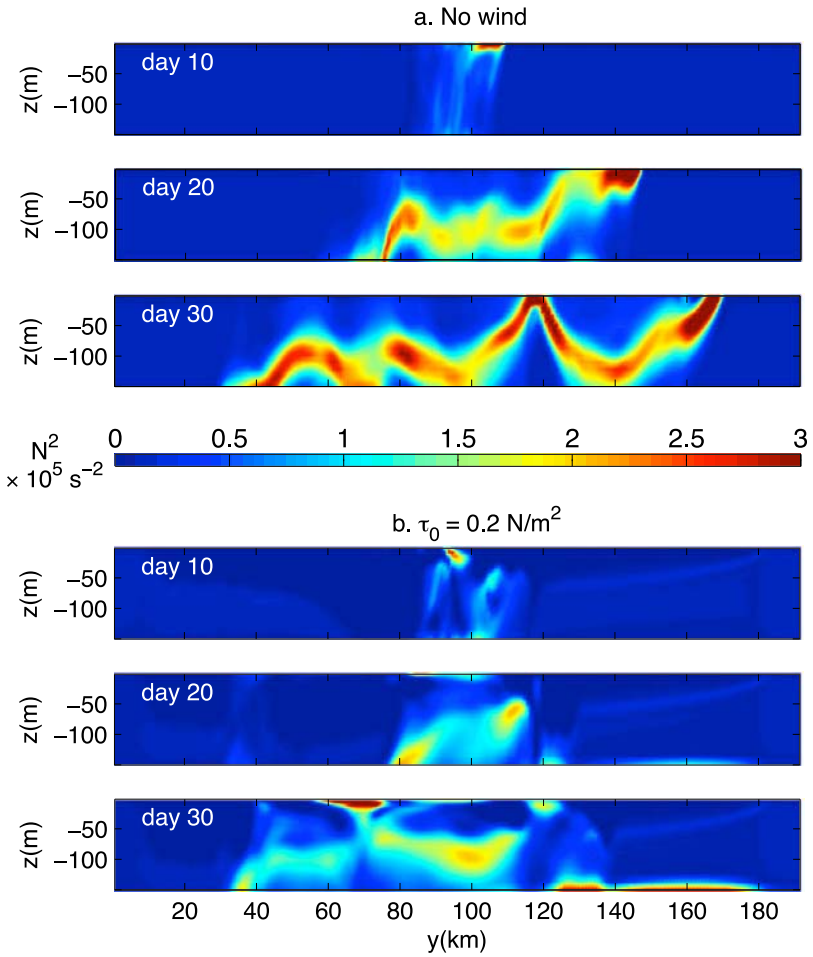

Figure 2. Across-channel sections showing a time sequence of buoyancy frequency N^2 within the ML for two cases: (a) no wind and (b) $\tau_0 = 0.2$ N m^{-2}. Lighter water is on the left, denser water on the right. The geostrophic current and down-front wind act outward from the plane of the figure. The images correspond to the times and cases shown in Figure 1. There is significant development of stratification in the middle of the ML when down-front winds are not present. With the down-front wind stress of 0.2 N m^{-2}, the growth of MLE and development of stratification are curtailed.

wind-driven secondary circulation in comparison to the MLE. In Figures 1b and 2b we show a simulation starting with the same density front as above but forced with a down-front wind stress of 0.2 N m^{-2}. While the onset of baroclinic instability is quicker, the spin down of the front is arrested (Figure 1b). The eddies are more vigorous than in the case without winds (Figure 3c), but they cannot restratify the ML over a wide region because their growth is arrested and Ekman advection of heavier water over light across the front keeps the isopycnals upright. In this case, mixing is triggered by the winds [*Thomas*, 2005], but other processes that enhance mixing, such as the loss of buoyancy at the surface, would act similarly to prevent stratification. When the wind is turned off (or reversed to act up front), the simulations show that frontal meandering and MLE grow in amplitude and rapidly restratify the mixed layer.

[21] The lateral distribution in the enhancement of mixed layer stratification is modulated by the eddies. While they draw stratified water from beneath the mixed layer, they also advect the stratification laterally, resulting in the shoaling of the mixed layer. Figure 4 shows the average N^2 in the upper 100 m of the mixed layer as it evolves in time. Figure 4 shows the lateral extent in ML stratification, but the stratification is not evenly distributed through the mixed layer. Rather, N^2 is concentrated middepth, as seen in Figure 2. When there is no wind forcing, the submesoscale MLE grow freely and occupy the lateral extent of the domain. When the wind is down front ($\tau = 0.2$ N m^2) and sufficient to arrest spin down, the MLE and the ensuing restratification do not perpetuate beyond the region occupied by the front.

[22] The development of the front from the initially straight initial configuration can be described in three phases. The first is leading up to the onset of instability, until which there are no MLE or restratification. In the second phase, the front develops meanders, whereby the alignment of the wind with the frontal axis is disrupted. Consequently, the wind-driven buoyancy flux is diminished and the eddies gain ground in restratifying. In the third phase, the spin down of the front by MLE results in a weakening of the eddy-driven circulation.

[23] The domain-wide, depth-averaged stratification of the mixed layer increases linearly in time for the case with

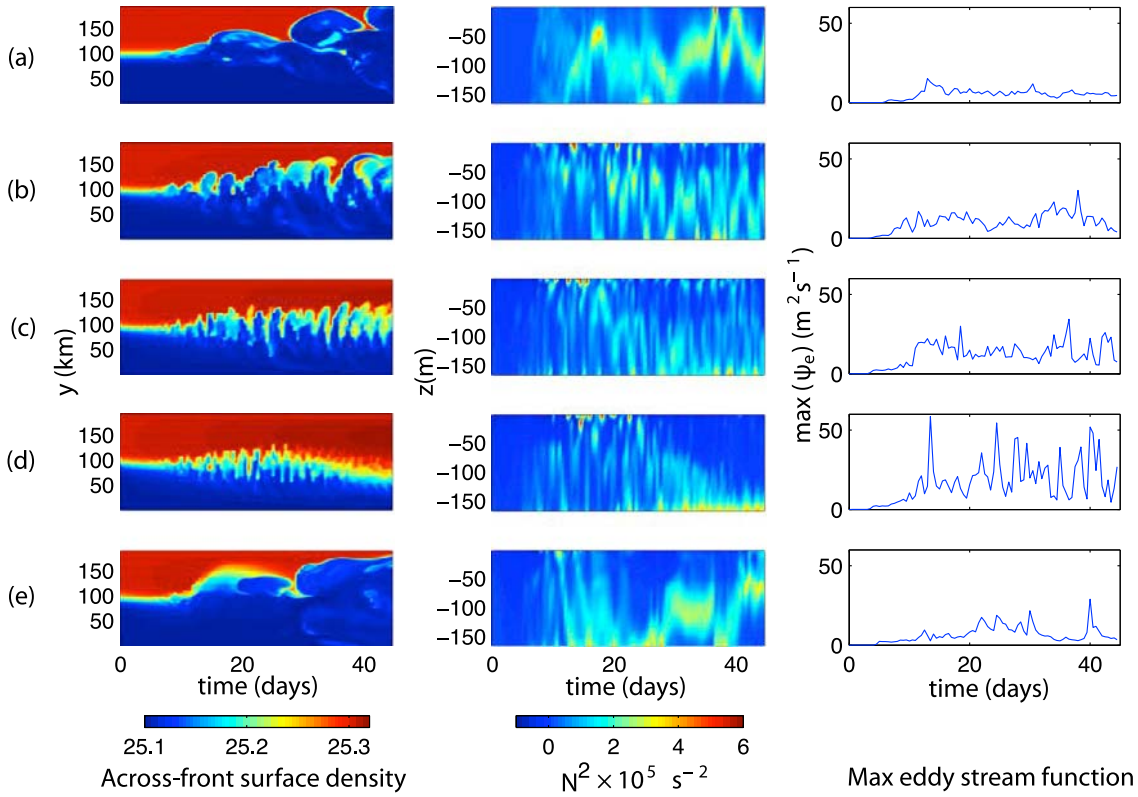

Figure 3. (left) Hovmoller diagram of the surface across-front density along a midchannel section, (middle) vertical profile of N^2 at the center of the domain, and (right) time series of the maximum eddy stream function ψ_e within the ML. Five different cases are compared from top to bottom: (a) no wind; (b) τ_0 = 0.1 N m^{-2}; (c) τ_0 = 0.2 N m^{-2}; (d) τ_0 = 0.3 N m^{-2}; and (e) τ_0 = 0.2 sin (π t/10) N m^{-2}, where t is given in days. The wind stress is sinusoidal in y and is tapered to 0 at the boundaries. In Figures 3b–3d, the wind is constant; in Figure 3e it varies sinusoidally between down front and up front every 10 days. The restratification by MLE proceeds uninhibited in the absence of winds (Figure 3a) and is aided by light water being transported over denser water when the wind stress is up front in Figure 3e. In the case of down-front winds, the MLE become more intense as the wind stress is increased, until an equilibrium is reached between wind-driven destratification and eddy-driven restratification (Figures 3c and 3d).

no winds (r = 0) until the stratification occurs throughout the domain. When $\tau_0 \geq 0.2$ N m^2 (i.e., $r \geq 1$), MLE grow following the initial spin-up phase and weaken the wind-driven buoyancy transport by meandering the front. The growth of MLE is arrested after about 10 days. The mean stratification plateaus and then decreases slightly as the down-front wind stress destratifies the mixed layer (Figure 5a).

[24] The competition between down-front winds and MLE is best illustrated via diagnosis of the mean and eddy overturning stream functions. We can diagnose the eddy stream function ψ_e as defined in (2). Similarly, $\overline{\psi}$ is computed from the x-averaged u and w fields. In the absence of wind forcing, $\overline{\psi}$ exhibits the characteristic ageostrophic circulation associated with a surface front: upward on the light side, downward on the dense side. This circulation is thermally direct but insignificant in magnitude as compared to ψ_e. The thermally direct ψ_e is what leads to rapid restratification at the front. Since there is nothing to inhibit the restratification of the ML, it proceeds rapidly after the onset of ML instability.

[25] When the wind blows down front, it sets up a thermally indirect circulation $\overline{\psi}$ over the entire cross-sectional area of the channel, which scales with the magnitude of the wind stress. The eddy-induced overturning stream function ψ_e, on the other hand, tends to be intense and localized at the front. In Figure 6, we plot $\overline{\psi}$ and ψ_e for the case when the down-front wind stress τ_0 = 0.2 N m^{-2}. The scaling discussed at the beginning of this section suggests that both $\overline{\psi}$ and ψ_e be approximately 2 m^2 s^{-1}. In Figure 6, ψ_e computed from the fully three-dimensional simulations shows a lot of variability, with maximum values exceeding 2 m^2 s^{-1} and negative values appearing where b_y changes sign. However, averaged over the frontal region, ψ_e has an average of about 2 m^2 s^{-1} at middepth in the ML. So does $\overline{\psi}$. The two countercirculations $\overline{\psi}$ and ψ_e have opposite signs on average and largely cancel each other, preventing restratification. The effective buoyancy flux and destratification tendency due to $\overline{\psi}$ further depends on the alignment of the wind with the frontal axis, which can meander substantially.

[26] When an up-front wind stress is applied to the model, restratification proceeds faster. Light water moves over dense water because of surface Ekman transport, capping the surface in a thin stratified layer. In this situation, MLE continue to act within the ML, but $\overline{\psi}$ and ψ_e are both ther-

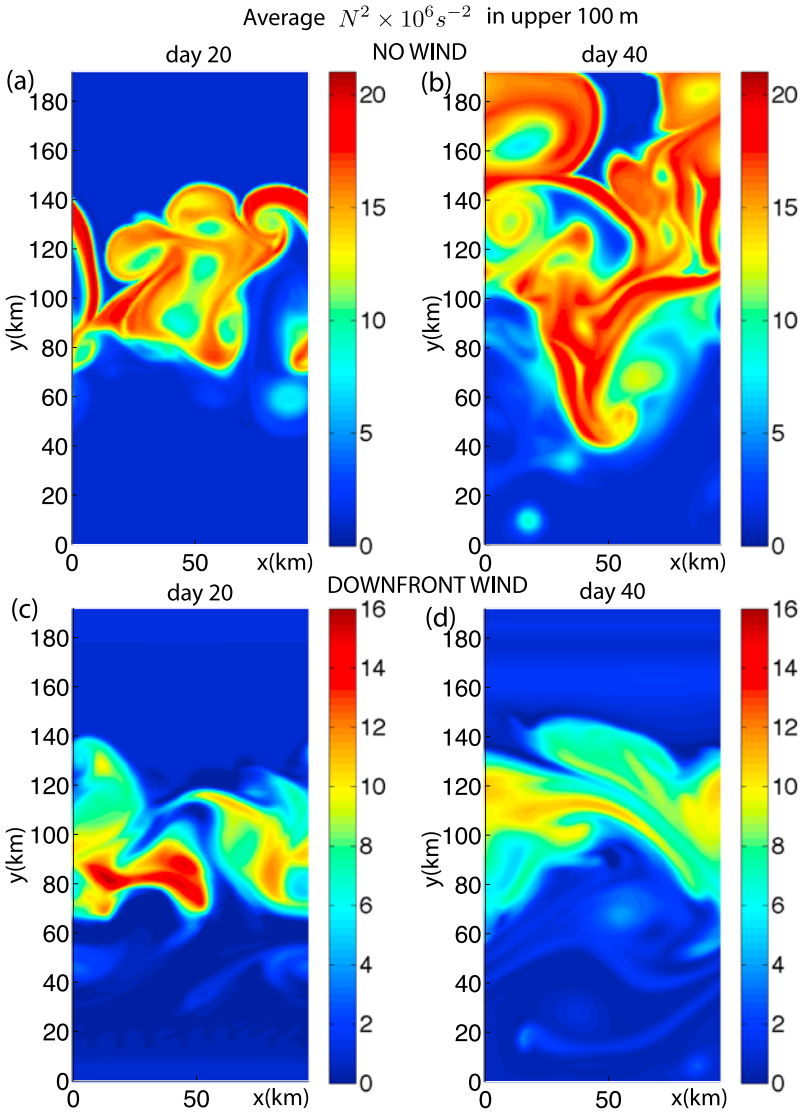

Figure 4. The average N^2 in the upper 100 m is shown at two different times: (left) 20 days and (right) 40 days after initialization, for (a and b) the cases without any wind forcing and for (c and d) down-front wind stress $\tau_0 = 0.2$ N m^2. In Figures 4c and 4d, the development of MLE is inhibited, and neither the MLE nor the stratification extend beyond a narrow region. The stratification is also weaker. This spatial view of the average N^2 in the upper 100 m should be viewed in conjunction with Figure 2, which shows its vertical distribution.

mally direct and reinforce each other to hasten the rate of restratification.

[27] The eddy overturning stream function represents the skew flux of buoyancy, $\mathbf{F}_{\text{skew}} \equiv \psi_e \hat{\mathbf{x}} \times \nabla b$, i.e., the along-isopycnal buoyancy flux associated with MLE. The skew flux accounts for the bulk of the eddy flux of buoyancy $\overline{\mathbf{u}'b'}$; the residual flux $\mathbf{F}_{\text{res}} = \overline{\mathbf{u}'b'} - \mathbf{F}_{\text{skew}}$ is largely diapycnal and represents the diabatic mixing across the front driven by MLE. Figure 7 shows the full, skew, and residual fluxes for one instance of time in the simulation with a down-front wind stress of $\tau_0 = 0.2$ N m^{-2}. In general, $\mathbf{F}_{\text{res}}$ is smaller than the full flux. This particularly holds where $\overline{b}_y$ is positive. However, where $\overline{b}_y$ is negative, ψ_e becomes large and the skew flux does not capture the bulk of the full flux, leaving a large residual flux. The residual mean decomposition proves to be useful in separating the advective and non-advective components of the eddy fluxes and thereby understanding the contribution of MLE to the buoyancy budget.

[28] To understand the effect of variable wind forcing on the restratification of a mixed layer front, we compare the time evolution of the front for simulations forced with different wind strengths. In Figure 3 we show the development of the across-front surface density and the stratification N^2 for five different wind stresses. When the winds are up front, absent, or weak, MLE slump the isopycnals, and light water overrides the denser water lying to the north of the front (Figures 3a and 3e, left). A similar evolution is seen in experiments with ML depths varying between 50 and 300 m but with a delayed onset and diminished strength of ψ_e for the shallower ML depths as anticipated from the linear stability theory [*Fox-Kemper et al.*, 2008]. With a sustained

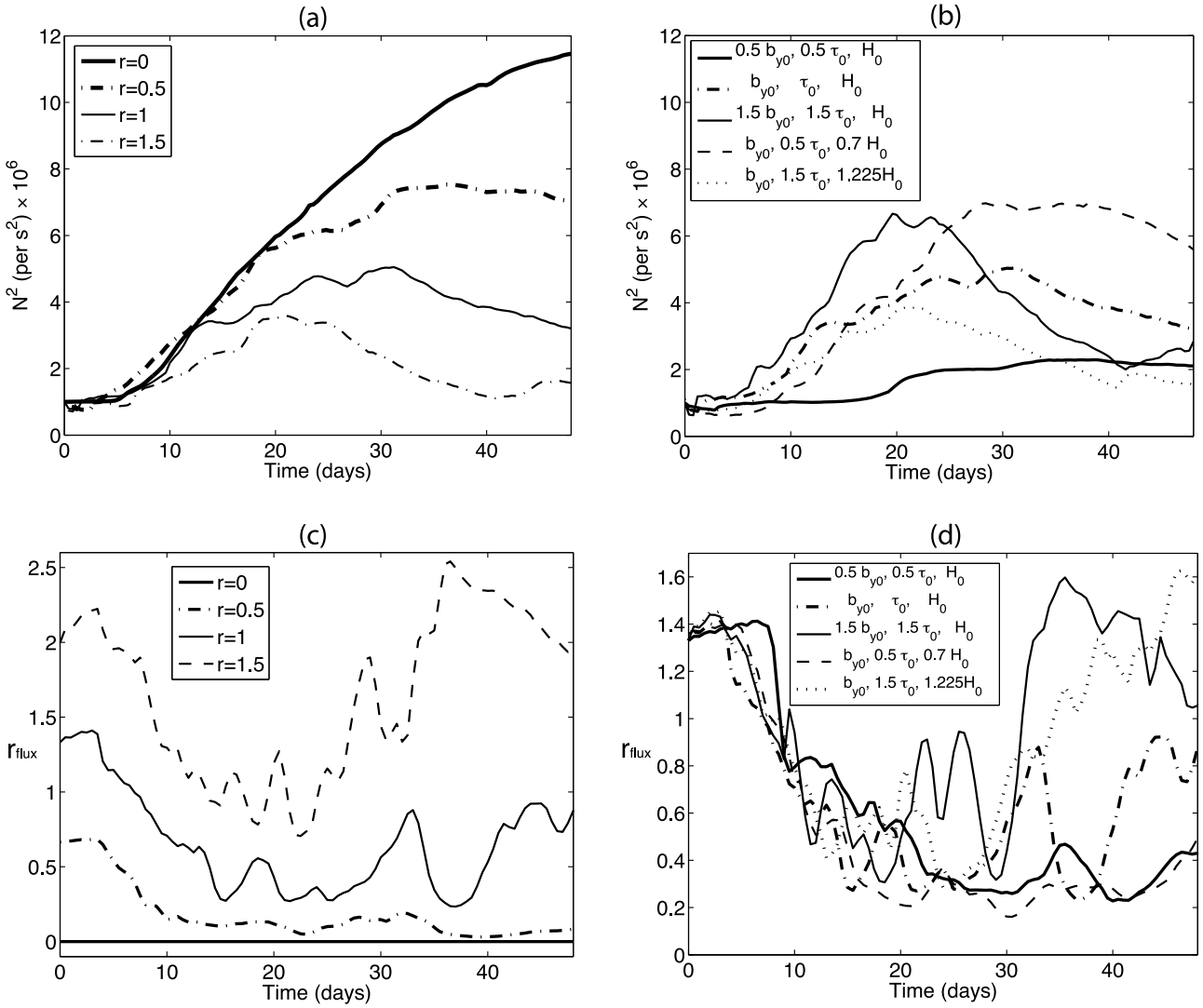

Figure 5. (top) The time evolution of the average domain-wide N^2 in the region above the isopycnal (σ = 25.4) at the base of the mixed layer. (a) Model simulations in which r is varied between 0 and 1.5 by increasing the strength of the down-front wind stress, where τ_0 = 0 N m^2, τ_0 = 0.1 N m^2, τ_0 = 0.2 N m^2, and τ_0 = 0.3 N m^2. When $r \geq 1$, the growth of MLE is arrested and N^2 can be seen to plateau and then decrease slightly. When r = 0, the MLE grow and the region-wide N^2 increases until the eddies reach the end of our model domain. (b) Model simulations in which r = 1, but the parameters τ, b_y, and H are varied as indicated in Table 1. In four of the five cases, the lateral extent of the ML stratification is arrested along with the growth of MLE. The ML N^2 then diminishes because of the destruction of stratification by down-front winds and mixing. When b_y is weak, the growth of the instability is slow and increase in mean N^2 is more gradual. (bottom) The value of r_{flux} calculated from surface averages estimates the relative strength of the wind- to eddy-driven buoyancy flux for the cases shown in (c) Figures 5a and (d) 5b. After an initial spin-up phase, r_{flux} is seen to decline as the effective cross-front, wind-driven transport is reduced because of the meandering of the front and its misalignment with the wind. Later, r_{flux} increases again. The decrease and increase in r_{flux} explain the increase and decrease in stratification.

down-front wind stress, the slumping of isopycnals by MLE is countered by the wind-driven secondary overturning. Light water does not cap off the denser water at the surface (Figures 3b–3d, left), particularly with more intensified down-front winds. Stratification by MLE does occur within the ML even when winds are down front (Figures 3b–3d, middle), largely because the effective transport of buoyancy by the wind-driven overturning is lessened as the front meanders and loses alignment with the wind direction in many locations. However, the stratification gained in the presence of down-front winds is transient, curtailed to the frontal region, and later eroded as the effect of the winds picks up over MLE (Figures 3a and 3e, middle).

[29] Our numerical simulations show that the maximum ψ_e in the y-z plane increases with the strength of the down-front wind (Figure 3). Down-front winds generate an

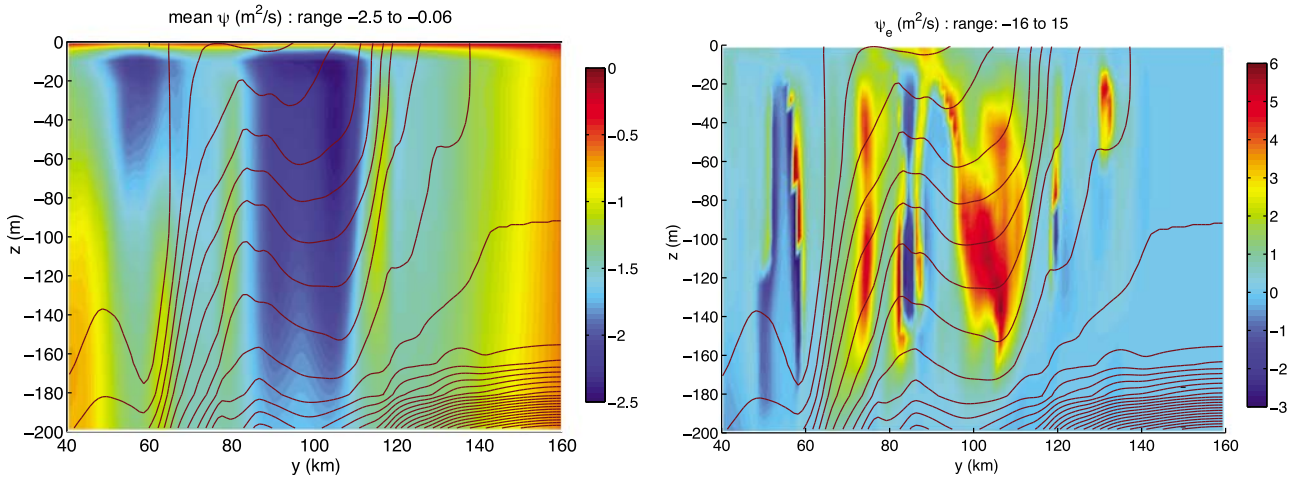

Figure 6. Comparison of the (a) $\overline{\psi}$ and (b) ψ_e on day 20 of the simulation with a down-front wind stress of 0.2 N m^{-2}. Here $\overline{\psi} = -\int \overline{v}\, dz = \int \overline{w}\, dy$ captures the wind-driven overturning, while the eddy stream function ψ_e is calculated according to equation (2). Though ψ_e has a some large localized extrema (as indicated by the range) and becomes negative where b_y changes sign, it has an average value of 2 m^2 s^{-1} middepth in the ML over the frontal region (y = 60 km and y = 130 km). The residual $\psi_r = \overline{\psi} + \psi_e$, which resembles ψ_e, is what drives the evolution of the mean fields. The contours denote isopycnals. Figure 6 shows only the ML and the frontal portion of the domain, which extends to 500 m in the vertical and 192 km in the y direction.

overturning circulation that opposes the slumping of the front. For sufficiently strong winds ($\tau_0 \geq 0.2$ N m^{-2}), an equilibrium is achieved between the supply of available potential energy (APE) supplied by the wind-driven upright mixing and the release of APE by MLE. This explains why MLE become more energetic for stronger winds; they can tap a larger supply of APE.

[30] The effect of MLE on the stratification of the ML can be conveniently expressed in terms of the surface heat gain Q, which would generate the same stratification. Unlike heating, which changes the mean buoyancy, MLEs change N^2 by redistributing buoyancy. Yet for comparison with other situations, we calculate Q as the vertical flux of density $\langle w\rho' \rangle$, where $\langle\ \rangle$ denotes averaging over a horizontal surface at middepth in the ML, and $\rho' = \rho - \langle \rho \rangle$. $Q = (C_p/\alpha)\langle w\rho' \rangle$, where α is the thermal expansion coefficient and C_p is the specific heat capacity of water. For the case without winds, the eddy-driven vertical fluxes of buoyancy generate Q that is O(100 W m^{-2}) averaged over the frontal region, with peak values of O(1000 W m^{-2}) at the front. This is comparable in magnitude (though opposite in sign) to the Q acting to reduce stratification when a strong down-front wind stress acts along a front [*Thomas*, 2005].

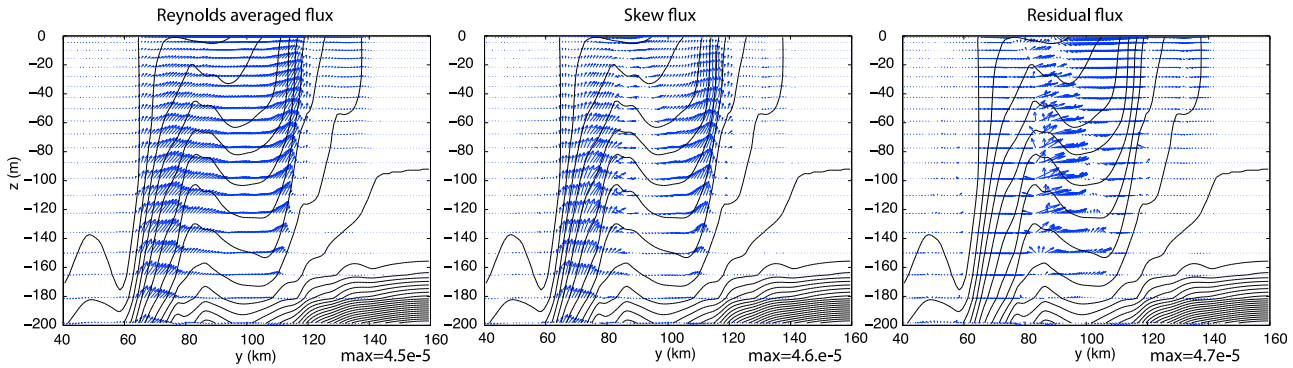

Figure 7. (left) The Reynolds flux of buoyancy $\overline{\mathbf{F}} = (\overline{v'b'}, \overline{w'b'})$ is resolved into (middle) the skew (or advective) buoyancy flux $\mathbf{F}_{\text{skew}} \equiv \psi_e \hat{\mathbf{x}} \times \nabla b$, which acts along isopycnals, and (right) the residual flux $\overline{\mathbf{F}}_{\text{res}}$, which is diapycnal and transports buoyancy down gradient. These fluxes are calculated for day 20 of the simulation with a down-front wind stress of 0.2 N m^{-2}. The corresponding value of ψ_e is shown in Figure 3. Contours denote isopycnals. As in Figure 3, only the ML and the frontal portion of the domain are shown.

Table 1. Experiments Performed in the Domain of 96 km × 192 km × 0.5 km at 1 km Horizontal Resolution[a]

b_y	H	τ	r
		Varying r	
b_{y0}	H_0	0	0
b_{y0}	H_0	$0.5\tau_0$	0.5
b_{y0}	H_0	τ_0	1
b_{y0}	H_0	$1.5\tau_0$	1.5
b_{y0}	H_0	$\tau_0 \sin(0.1\pi\ t)$	1.5
		$r = 1$	
$0.5b_{y0}$	H_0	$0.5\tau_0$	1
b_{y0}	H_0	τ_0	1
$1.5b_{y0}$	H_0	$1.5\tau_0$	1
b_{y0}	$0.7H_0$	$0.5\tau_0$	1
b_{y0}	$1.225H_0$	$1.5\tau_0$	1

[a]All parameters are varied with respect to the baseline values $b_{y0} = 0.9 \times 10^{-7}$ s^{-2}, $H_0 = 200$ m, and $\tau_0 = 0.2$ N m^{-2}. Negative τ indicates that the wind is up front. The parameter $r \equiv |\overline{\psi}/\psi_e| = \tau_0/(0.06\rho H^2\overline{b_y})$ is the ratio of the strength of the mean wind-driven to eddy-driven overturning circulations.

[31] The parameter $r \equiv |\overline{\psi}/\psi_e| = \tau_0/(0.06\rho H^2\overline{b_y})$ is a measure for the relative strength of wind forcing compared to MLE. To assess the variations that may result from individual parameters, we perform another set of numerical experiments wherein we maintain a constant value of $r = 1$ while varying the parameters b_y, H, and τ_0 as shown in Table 1. Since $r = 1$, the MLE do not grow in size and overrun the entire domain; the front is maintained (Figure 8) in spite of the different combinations of individual parameters, as expected from the scaling arguments. Figure 5b shows the development of N^2 for five different cases with $r = 1$. While the response is common in the gross sense, the details of N^2 development differ and depend on the parameter b_y over and above its effect on r. One reason is that the ratio of the wind- and eddy-driven transport of buoyancy varies as reflected by r_{flux} in Figure 5d.

[32] The results of our analysis support the need for an advective parameterization for MLE in models that are unable to resolve submesoscales and raise the question as to whether the parameterization of *Fox-Kemper et al.* [2008] can be applied even in the presence of wind forcing. Presumably, a coarse resolution model would be able to capture

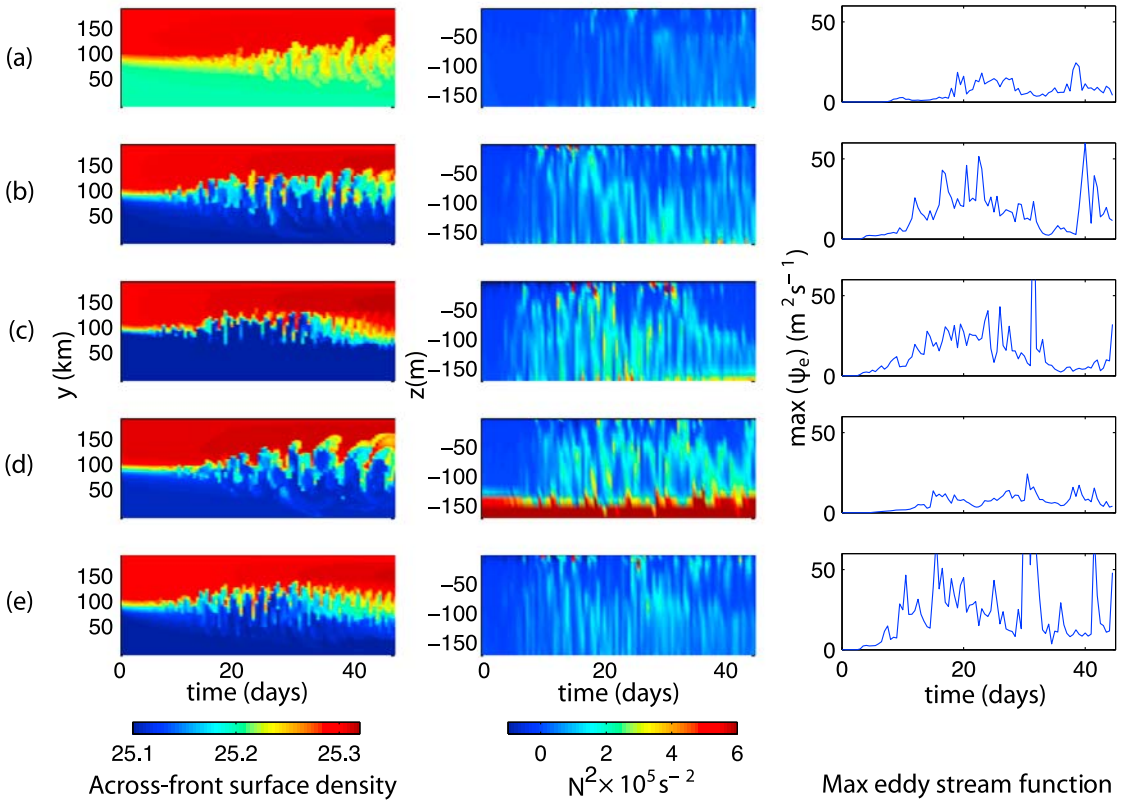

Figure 8. (left) Hovmoller diagram of the surface across-front density along a midchannel section, (middle) vertical profile of N^2 at the center of the domain, and (right) time series of the maximum eddy stream function ψ_e within the ML, just as shown in Figure 3 but where $r = 1$ for all the cases. The parameters b_y, H, and τ_0 are varied with reference to the baseline parameters $b_{y0} = 0.9 \times 10^{-7}$ s^{-2}, $H_0 = 200$ m, and $\tau_0 = -0.2$ N m^{-2} (see Table 1) as follows for the five cases shown from top to bottom: (a) $0.5b_{y0}$, H_0, $0.5\tau_0$; (b) b_{y0}, H_0, τ_0; (c) $1.5b_{y0}$, H_0, $1.5\tau_0$; (d) b_{y0}, $0.7H_0$, $0.5\tau_0$; and (e) b_{y0}, $1.225H_0$, $1.5\tau_0$. In all the cases, the front maintains its position and the development of MLE and stratification is restricted to a relatively narrow region as compared to the case where $r < 1$ (Figure 5).

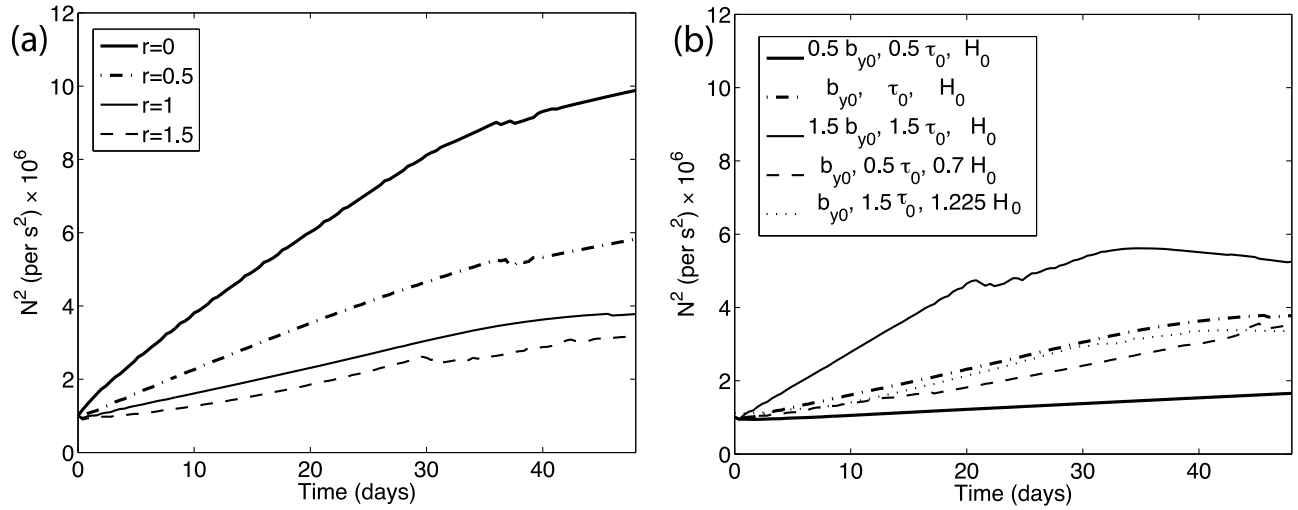

Figure 9. The time evolution of the average domain-wide N^2 for a two-dimensional version of the model with the parameterization for MLE [*Fox-Kemper et al.*, 2008]. N^2 is averaged in the region above the isopycnal ($\sigma = 25.4$), which forms the base of the mixed layer. The x-averaged equations are integrated in time with wind forcing, and the ψ_e to be parameterized is evaluated and added to the mean circulation in the advection of buoyancy. (a) For model simulations in which r is varied between 0 and 1.5, we vary the strength of the down-front wind stress as follows: $\tau_0 = 0$ N m^2, $\tau_0 = 0.1$ N m^2, $\tau_0 = 0.2$ N m^2, and $\tau_0 = 0.3$ N m^2. The parameterization captures the gross response of the mixed layer even in the presence of wind forcing. (b) For model simulations in which $r = 1$ is held constant, the parameters τ_0, b_y, and H are varied as indicated in Table 1. Even though r based on the initial conditions is the same in all cases, N^2 is not independent of the frontal evolution and individual values of the parameters. The cases where b_y is weaker or stronger differ from the other three.

the wind-driven circulation $\overline{\psi}$, while ψ_e can be parameterized and added to the mean circulation to account for the advection of buoyancy by unresolved submesoscale eddies. To test this, we integrate the x-averaged version of the model equations within the same numerical framework and with the same initial conditions and wind forcing as was used for the three-dimensional model. This enables us to take into account the along-front average effect of wind on the mean secondary circulation. We use a horizontal grid spacing of 4 km, whereas the vertical grid spacing is the same as in the 3-D case. The parameterization for the eddy-driven overturning stream function $\psi_e \sim 0.06\, H^2 \overline{b}_y / f$ [*Fox-Kemper et al.*, 2008] is evaluated locally in space (b_y is local in space, but H is its initial value and is held constant) at every time step and is applied along with the mean wind-driven overturning to the advection of buoyancy. These simulations with wind forcing are run for all the cases shown in Table 1. The two-dimensional mean circulation with the eddy parameterization is able to roughly capture differences in the evolution of stratification for changing r (Figure 9a), but the increase in N^2 is not arrested in the way that it is in the 3-D model. For the simulations with $r = 1$ (Figure 9b), the evolution of the mean N^2 is not entirely independent of the values of individual parameters; the runs with a different value of b_y are dissimilar. Further work is needed to understand these differences. In the case of small-amplitude eddies, the mean circulation would be largely wind driven, but for larger eddies, the rectified effect is likely to change the mean. Thus, considering the evolution over long times, this may be the reason for some of the differences. Further, MLE have a positive feedback. As they disrupt the alignment of the wind and frontal axis, they reduce the effective buoyancy transport achieved by the wind.

5. Conclusions

[33] Eddies ensuing from baroclinic instability within the ML can restratify the ML and increase its mean N^2 within a few days. The restratification occurs through the spin down of the front and is supported by eddy fluxes of highly stratified water from the underlying pycnocline and frontogenesis arising from the surface expression of the MLE. It can, however, be countered by a down-front wind stress at the surface, which arrests the spin down of the front and acts to destratify the ML. When sufficiently strong, the down-front wind can maintain the isopycnals at the front as nearly vertical and consequently can arrest the enhancement of stratification by MLE over long periods. In this situation, potential energy input by the wind is extracted by strengthened MLE, and an equilibrium is achieved between the two processes. Conversely, restratification is speeded up when the wind stress is up front.

[34] The framework of the residual overturning stream function is useful for diagnosing the along- and cross-isopycnal fluxes of buoyancy induced by the submesoscale MLE. The net advective buoyancy flux is the sum of the advective effect of eddies and the mean wind-driven circulation. The scaling estimate for the eddy stream function captures the average eddy advection in the simulations and can be compared to the wind-driven overturning to determine whether or not restratification will occur. Parameterization of the thermally direct circulation induced by

submesoscale eddies in the presence of wind forcing is required in climate models in order to simulate the restratification correctly.

[35] Application of the parameterization of *Fox-Kemper et al.* [2008] to an along-front averaged version of the model with wind forcing qualitatively captures the integrative effect of wind and the eddy-driven circulations on the development of stratification at a front. Restratification by the eddy-driven circulation is slowed down by the superposition of a counteracting wind-driven overturning.

[36] **Acknowledgments.** We acknowledge the generous support of NSF through awards OCE-0623264 (A.M. and A.T.) and OCE-0612143 (R.F.).

References

Andrews, D., and M. E. McIntyre (1976), Planetary waves in horizontal and vertical shear: The generalized Eliasen-Palm relation and the mean zonal acceleration, *J. Atmos. Sci.*, *33*, 2031–2048.

Boccaletti, G., R. Ferrari, and B. Fox-Kemper (2007), Mixed layer instabilities and restratification, *J. Phys. Oceanogr.*, *37*, 2228–2250.

Capet, X., J. C. McWilliams, M. J. Molemaker, and A. F. Shchepetkin (2008a), Mesoscale to submesoscale transition in the California Current system. Part I: Flow structure, eddy flux, and observational tests, *J. Phys. Oceanogr.*, *38*, 29–43.

Capet, X., J. C. McWilliams, M. J. Molemaker, and A. F. Shchepetkin (2008b), Mesoscale to submesoscale transition in the California Current system. Part II: Frontal processes, *J. Phys. Oceanogr.*, *38*, 44–64.

Cerovecki, I., R. A. Plumb, and W. Heres (2009), Eddy transport and mixing on a wind- and buoyancy-driven jet on the sphere, *J. Phys. Oceanogr.*, *39*, 1133–1149, doi:10.1175/2008JPO3596.1.

Ferrari, R., J. McWilliams, V. Canuto, and D. Dubovikov (2008), Parameterization of eddy fluxes at the ocean boundaries, *J. Clim.*, *31*, 2770–2789.

Fox-Kemper, B., and R. Ferrari (2008), Parameterization of mixed layer eddies. Part II: Prognosis and impact, *J. Phys. Oceanogr.*, *38*, 1166–1179.

Fox-Kemper, B., R. Ferrari, and R. Hallberg (2008), Parameterization of mixed layer eddies. Part I: Theory and diagnosis, *J. Phys. Oceanogr.*, *38*, 1145–1165.

Gent, P., and J. McWilliams (1990), Isopycnal mixing in ocean circulation models, *J. Phys. Oceanogr.*, *20*, 150–155.

Green, J. S. (1970), Transfer properties of the large-scale eddies and the general circulation of the atmosphere, *Q. J. R. Meteorol. Soc.*, *96*, 157–185.

Held, I. M., and T. Schneider (1999), The surface branch of the zonally averaged mass transport circulation in the troposphere, *J. Atmos. Sci.*, *56*, 1688–1697.

Hosegood, P., M. Gregg, and M. Alford (2006), Sub-mesoscale lateral density structure in the oceanic surface mixed layer, *Geophys. Res. Lett.*, *33*, L22604, doi:10.1029/2006GL026797.

Lapeyre, G., P. Klein, and B. L. Hua (2006), Oceanic restratification forced by surface frontogenesis, *J. Phys. Oceanogr.*, *36*, 1577–1590.

Lee, C., E. D'Asaro, and R. Harcourt (2006), Mixed layer restratification: Early results from the AESOP program, *EOS Trans. AGU*, *87*(52), Fall Meet. Suppl., Abstract OS51E-04.

Mahadevan, A. (2006), Modeling vertical motion at ocean fronts: Are nonhydrostatic effects relevant at submesoscales?, *Ocean Modell.*, *14*, 222–240.

Mahadevan, A., J. Oliger, and R. Street (1996a), A nonhydrostatic mesoscale ocean model. Part I: Well-posedness and scaling, *J. Phys. Oceanogr.*, *26*, 1168–1880.

Mahadevan, A., J. Oliger, and R. Street (1996b), A nonhydrostatic mesoscale ocean model. Part 2: Numerical implementation, *J. Phys. Oceanogr.*, *26*, 1181–1900.

Marshall, J., and T. Radko (2003), Residual mean solutions for the Antarctic Circumpolar Current and its associated overturning circulation, *J. Phys. Oceanogr.*, *33*, 2341–2354.

Plumb, R. A. (2002), Stratospheric transport, *J. Meteorol. Soc. Jpn.*, *80*, 793–809.

Plumb, R. A., and R. Ferrari (2005), Transformed Eulerian-mean theory. Part I: Nonquasigeostrophic theory for eddies on a zonal-mean flow, *J. Phys. Oceanogr.*, *35*, 165–174.

Spall, M. (1995), Frontogenesis, subduction, and cross-front exchange at upper ocean fronts, *J. Geophys. Res.*, *100*(C2), 2543–2557.

Tandon, A., and C. Garrett (1994), Mixed layer restratification due to a horizontal density gradient, *J. Phys. Oceanogr.*, *24*, 1419–1424.

Tandon, A., and C. Garrett (1995), Geostrophic adjustment and restratification of a mixed layer with horizontal gradients above a stratified layer, *J. Phys. Oceanogr.*, *25*, 2229–2241.

Thomas, L. N. (2005), Destruction of potential vorticity by winds, *J. Phys. Oceanogr.*, *35*, 2457–2466.

Thomas, L. N., and R. Ferrari (2008), Friction, frontogenesis, and the stratification of the surface mixed layer, *J. Phys. Oceanogr.*, *38*, 2501–2518.

Thomas, L., and C. Lee (2005), Intensification of ocean fronts by down-front winds, *J. Phys. Oceanogr.*, *35*, 1086–1102.

Thomas, L., A. Tandon, and A. Mahadevan (2008), Submesoscale processes and dynamics, in *Ocean Modeling in an Eddying Regime*, *Geophys. Monogr. Ser.*, vol. 177, edited by M. Hecht and H. Hasumi, pp. 17–38, AGU, Washington, D. C.

Weller, R. A., P. W. Furey, M. A. Spall, and R. E. Davis (2004), The large-scale context for oceanic subduction in the northeast Atlantic, *Deep Sea Res., Part I*, *51*, 665–699.

R. Ferrari, Department of Earth, Atmospheric, and Planetary Sciences, MIT, Bldg. 54, Rm. 1420, 77 Massachusetts Ave., Cambridge, MA 02139, USA.

A. Mahadevan, Department of Earth Sciences, Boston University, 685 Commonwealth Ave., Rm. 127, Boston, MA 02215, USA.

A. Tandon, Department of Physics, University of Massachusetts Dartmouth, 285 Old Westport Rd., North Dartmouth, MA 02747, USA.